JOURNAL OF Materials CHEMISTRY

Behaviour of the one-dimensional, inorganic polymer $^1_\infty[MPS_4]^-$ anions (M = Ni, Pd) in organic solutions†

Julien Sayettat,[a] Lucy M. Bull,[a] Stéphane Jobic,[a] Jean-Christophe P. Gabriel,[a] Marc Fourmigué,[a] Patrick Batail,*[a] Raymond Brec,*[a] René-Louis Inglebert[b] and Claude Sourisseau[c]

[a]*Institut des Matériaux de Nantes, UMR 6502 CNRS-Université de Nantes, BP 32229, 44322 Nantes, France. Fax: +33 (0)2 40 37 39 95. E-mail: lastname@cnrs-imn.fr*
[b]*GREMI, UFR Faculté des Sciences, rue de Chartres, BP 6759, 45067, Orléans Cedex 2, France, and CBN-CNRS, rue Ch. SADRON, 45071, Orléans Cedex 2, France*
[c]*Laboratoire de Physicochimie Moléculaire, Université Bordeaux I, 351 cours de la Libération, UMR 5803, 33405, Talence, France*

Received 28th May 1998, Accepted 24th July 1998

The behaviour of the $KMPS_4$ (M = Ni, Pd) salts and some solid-solution phases, $KNi_xPd_{1-x}PS_4$, when dissolved in dimethylformamide (DMF) have been studied. For $KNiPS_4$–DMF the novel re-arranged molecular bowl-like $[Ni_3P_3S_{12}]^{3-}$ trianion can be formed from solutions that have been heated at 323 K for 2 days and K^+ exchanged by larger organic cations such as PPh_4^+ (tetraphenylphosphonium), TMA^+ (tetramethylammonium), TEA^+ (tetraethylammonium), and MEM^+ (methylethylmorpholinium). This remarkable dispersion/auto-fragmentation/re-arrangement sequence extends the concept of mere excision in solution of monomeric molecular motifs from low-dimensional inorganic solids. Investigations by electrospray mass spectrometry (ESMS), ^{31}P solution-state NMR and optical microscopy under polarized light of $KNiPS_4$ in DMF have shown that chains of $^1_\infty[MPS_4]^-$ exist intact in freshly prepared solutions. These solutions show transient birefringence under stress. ESMS and NMR studies of $KNiPS_4$ solutions show that the $^1_\infty[NiPS_4]^-$ chains are quickly broken down at ambient temperature and that cyclic $[Ni_3P_3S_{12}]^{3-}$ trianions are formed. By contrast, the $^1_\infty[PdPS_4]^-$ chain remains intact at temperatures up to 323 K. This behavioural difference can be understood in terms of the Ni–S and Pd–S bond strengths. ESMS spectra of aged $KNi_xPd_{1-x}PS_4$/DMF solutions indicate that mixed metal trianions are formed, such as $[Ni_2PdS_{12}]^{3-}$, $[NiPd_2P_3S_{12}]^{3-}$ and $[Ni_3P_3S_{12}]^{3-}$, but no $[Pd_3P_3S_{12}]^{3-}$ species have yet been observed.

Low dimensional compounds have been extensively investigated because of their fascinating properties that are inherent with their structural anisotropy.[1,2] These properties encompass, for example, charge density waves,[3–5] superconductivity[6,7] and low-dimensional magnetism.[8,9] Self assembly of such one- or two-dimensional compounds is common with chalcogenides, where the chains or layers are separated by a van der Waals gap. These compounds are stabilised by a combination of factors; strong transition metal–chalcogen interactions in the chains or layers, and, because of the low electronegativity of sulfur and selenium, relatively weak repulsions, in comparison to other systems such as oxides,[10,11] between the negatively charged chains or layers. In addition, these compounds may be stabilised by alkali or alkaline earth cations that can act as spacers between the chains or layers, ensuring electrostatic shielding between the negatively charged entities.[12,13]

The reactive flux method[14] using polychalcogenides AQ_x (A = alkali metal, Q = S, Se) has produced a wide variety of low dimensional, novel materials AM_yQ_x (M = transition metal and/or main group element). These new phases have been reviewed extensively.[15,16] It has been shown that depending upon the concentration and nature of the alkali metal, the dimensionality of the covalent framework can be controlled.[17–19] In general, a decrease of the covalent block dimensionality is expected upon progressive addition of alkali metal (changing the electrostatic interactions) or by substitution of a counter cation by a larger one (change in the steric factors). Such phenomena originate from a competition between A–Q ionic bonding and M–Q covalent bonding, with minimisation of the ionic–covalent interfacial energy.

In low dimensional solids the bonding anisotropy is reflected in the chemical reactivity.[11] Exchange reactions, by soft chemistry routes, of A in the AM_yQ_x phases may be envisioned to modify the separation between individual layers of chains, and/or to lead to new structural arrangements. Such a procedure has been developed recently to synthesise $(NEt_4)_2HgSnTe_4$ through the reaction of ethylenediamine with one-dimensional $K_2HgSnTe_4$ followed by a treatment with NEt_4I.[20] However, solvation of the A^+ cation by polar inorganic or organic solvents may also occur leading to the separation of the $M_yQ_x^-$ anionic entities. This is known as exfoliation. Such reactions may give rise to a complete dispersion of the AM_yQ_x compound, thus forming colloïdal solutions containing highly anisotropic particles.[21] The solubility of a low dimensional material in a particular solvent depends upon the lattice energy and the solvation energy of the alkali metal and anionic framework.[10,11] The latter is favoured by a high relative permittivity. The possibility to exfoliate or even dissolve mineral compounds is of major importance because it then allows modification of the solids by solution chemistry methods and paves the way to the synthesis of new organic–inorganic hybrid and nanocomposite materials. Furthermore, in some cases these solutions of mineral motifs can present mesogenic properties such as $^1_\infty[Mo_3Se_3]^-$, which has been demonstrated to be a liquid crystal with a mineral core when dispersed in DMF.[22]

Recently, we succeeded in synthesising new thiophosphates of nickel and palladium with the chemical formula $KMPS_4$ (M = Ni, Pd).[23,24] These isostructural compounds exhibit a marked one-dimensional character based on $^1_\infty[MPS_4]^-$ chains. Prompted by our interest in dissolving low dimensional mineral compounds, we show in this article that both phases are highly

†Basis of the presentation given at Materials Chemistry Discussion No. 1, 24–26 September 1998, ICMCB, University of Bordeaux, France.

soluble in polar organic solvents, and that the $^1_\infty[MPS_4]^-$ polymer in solution forms complex fluids.[25] For the case of $KNiPS_4$, the $^1_\infty[NiPS_4]^-$ chains dissolved in DMF undergo an auto-fragmentation/rearrangement process into an unprecedented concave $[Ni_3P_3S_{12}]^{3-}$ anion.[25] Mass spectrometry and solution-state nuclear magnetic resonance (NMR) have been used to characterize this process. In addition, taking advantage of the solution phase chemistry of $KNiPS_4$, four novel phases are obtained by cation exchange (metathesis) of the type $(A^+)_3[Ni_3P_3S_{12}]^{3-}$, A^+ = tetraethylammonium (TEA^+), tetraphenylphosphonium (PPh_4^+),[25] methylethylmorpholinium (MEM^+) and tetramethylammonium (TMA^+). $KPdPS_4$ does not show such a reactivity under similar conditions.

Experimental

Solid state synthesis

Isostructural $KNiPS_4$ and $KPdPS_4$ compounds were prepared as described previously.[23,24] $KNi_xPd_{1-x}PS_4$ solid solutions were prepared as for the $x=0$ and 1 members producing red, homogeneous powders, which were subsequently investigated by powder XRD (see below).

Solution chemistry

All dissolutions were carried out in air, at room temperature by stirring the $KMPS_4$–DMF solution (0.156 mmol l^{-1}) for a few hours. $KNiPS_4$ formed a very viscous, deep brown solution containing orange particles of undissolved solid. If this solution was heated at 323 K for two days, it became less viscous and more homogeneous. $(A^+)_3[(NiPS_4^-)_3]$ salts ($A^+ = PPh_4^+$ **1**,[25] TMA^+ **2**, TEA^+ **3**, MEM^+ **4**) were typically synthesized by adding a 1.87 mmol l^{-1} solution of AX (X = Cl, Br or I) in DMF to 10 ml of a two-day aged solution of $KNiPS_4$–DMF (0.156 mmol l^{-1}). After stirring this mixture for 30 min the product could be precipitated from the solution by adding diethyl ether, and recrystallized from acetonitrile (CH_3CN). Calculated (found) elemental analysis for: $C_{24}H_{20}P_2NiS_4$ **1**: C, 47.64 (47.95); H, 3.33 (3.71%); $C_7H_{16}ONNiPS_4$ **3**: C, 24.15 (23.46); H, 4.63 (4.48%); $C_4H_{12}NNiPS_4 \cdot 1/3CH_3CN$ **4**: C, 18.34 (17.30); H, 4.29 (4.13%). Electron microprobe analysis gave the following Ni : S : P ratio (EMPA was performed on flat crystalline surfaces, using a JEOL JSM-58LV electron microprobe equipped with a PGT IMIX-PTS energy dispersive spectrometer): 1 : 3.7 : 2 for **1**, 1 : 3.8 : 1 for **2**, 1 : 3.9 : 1 for **3** and 1 : 3.7 : 1 for **4**.

Single crystal X-ray diffraction

Crystallographic data, reported previously in the case of **1**,[25] were collected for samples **2**, **3** and **4** on a STOE image plate X-ray diffractometer. Data collections were performed at room temperature for all compounds, except for sample **3**, which was studied at 170 K because of the difficulties encountered in refining the positions of the organic cations from data collected at room temperature. The data were reduced to net intensities, estimated standard deviations were calculated on the basis of counting statistics, Lorentz polarisation corrections were applied, and equivalent reflections were averaged. The structures were solved from direct methods using SHELXTL[26] or SIR-92,[27] and they were refined with XTAL-34.[28] Final refinements were performed on F_o with anisotropic atomic displacement parameters for Ni, P, S, and isotropic ones for O, N and C. The hydrogen atomic positions were introduced in the calculations: they were not refined, but were assigned isotropic atomic displacement factors of 0.15 and 0.10 $Å^2$ for high and low temperature data recording, respectively. Moreover, aliphatic carbon–carbon, quaternary carbon nitrogen atoms and carbon–oxygen distances were constrained to be 1.54, 1.47 and 1.44 Å (with a tolerance factor of ± 0.01 Å), respectively. Finally, refinements by full matrix least squares methods on all the structures gave final R (R_{wF}) values of 0.048 (0.052), 0.068 (0.078) and 0.063 (0.074), for **2**, **3** and **4**, respectively. No significant residual peaks were observed in the final electron difference map with electron densities ranging between 0.66 and -0.45 e $Å^{-3}$. Table 1 gives details of the data collections and the results of the structural refinements. Cell parameters were determined from least squares refinements from the setting angles of 2000, 2000 and 214 reflections in the range $2.9 \leqslant 2\theta \leqslant 48.4°$ for samples **2**, **3** and **4**, respectively. The final atomic parameters and atomic displacement parameters of **2**, **3** and **4** are given in the CCDC data (see below). However, since the anion $[Ni_3P_3S_{12}]^{3-}$ is found systematically in all these phases the atomic coordinates of the Ni, P and S atoms for compound **1** (PPh_4NiPS_4), along with some selected distances, are given in Tables 2 and 3.

Full crystallographic details for samples **2**, **3** and **4**, excluding structure factors, have been deposited at the Cambridge Crystallographic Data Centre (CCDC). See Information for Authors, *J. Mater. Chem.*, 1998, Issue 1. Any request to the CCDC for this material should quote the full literature citation and the reference number 1145/114.

$KNi_xPd_{1-x}PS_4$ solid solution X-ray powder diffraction data

Powder diffraction diagrams were recorded in a Debye-Scherrer geometry on an INEL CPS 120 position sensitive detector in the 2θ range 0–120° (Cu-Kα_1 radiation and with $Na_2Ca_3AlF_{14}$ as standard). After grinding and sieving at 50 μm, the powders were introduced in 0.1 mm diameter Lindeman capillaries. The structural refinement was performed with the Rietveld program Fullprof.[29] Since no superstructure (arising from an ordering between Ni and Pd) was observed by electronic diffraction, the refinements were carried out using the structural data of the $KMPS_4$ structural type. Ni and Pd occupancy ratios were refined and the sum constrained to one. The three $KNi_xPd_{1-x}PS_4$ samples studied yielded x values of 0.22(3), 0.44(2) and 0.76(2). Results of these refinements are given in Table 4.

Electrospray mass spectroscopy (ESMS)

Experiments were carried out using a VG Quatro II triple quadrupole mass spectrometer (VG BioRech Ltd, Altrincham, UK). The spectra presented here result from an average of six mass scans, each one of 10 s (multi channel acquisition (MCA) mode in Mass Lynx program), then the data were smoothed by a Fourier transform filter. The mass peak half-width is practically constant for all the mass spectra ($m/z \approx 1$). The measurements were made for DMF solutions at a concentration of *ca.* 1.5×10^{-2} mol l^{-1}. The solvent evaporation in the spectrometer was assisted by a nitrogen flow heated at 343 K. For the interpretation of the spectra, only the transition metal and the potassium isotopes with isotopic abundances >5% have been considered: ^{31}P, 100%; ^{32}S, 95%; ^{34}S, 4%; ^{39}K, 93%; ^{41}K, 7%; ^{58}Ni, 68%; ^{60}Ni, 26%; ^{104}Pd, 11%; ^{105}Pd, 22%, ^{106}Pd, 27%; ^{108}Pd, 26%; ^{110}Pd, 12%. Moreover, only anionic entities with an abundance >10% are reported.

^{31}P solution-state NMR

Measurements were performed on a Bruker AM200 spectrometer operating at a frequency of 81 MHz. Spectra were collected with a *ca.* 20° pulse length of 2 μs and a recycle time of 3–5 s. No proton decoupling was used and so the relative intensities of the signals are quantitative. Processing of the data was performed using the PC version of WINNMR (Bruker). The measurements were performed on deuterated DMF solutions at a concentration of *ca.* 3×10^{-2} mol l^{-1}. This concentration allowed good signal/noise spectra to be

Table 1 Details of the data collections and refinement parameters for $A_3[Ni_3P_3S_{12}]$ compounds ($A^+ = PPh_4^+$ **1**, TMA^+ **2**, TEA^+ **3** and MEM^+ **4**)

Formula	$(C_{24}H_{20}P)_3Ni_3P_3S_{12}$ **1**	$(C_4H_{12}N)_3Ni_3P_3S_{12}\cdot CH_3CN$ **2**	$[C_8H_{20}N]_3Ni_3P_3S_{12}$ **3**	$(C_7H_{16}ON)_3Ni_3P_3S_{12}$ **4**
Molecular mass/g	1670.82	916.73	1043.1	1043.1
Space group	$P2_1/c$ (no. 14)	$P\bar{1}$ (no. 2)	$P2_1/c$ (no. 14)	$P\bar{1}$ (no. 2)
Cell parameters: a/Å	15.828(2)	14.494(1)	16.757(2)	12.076(1)
b/Å	10.099(1)	15.952(2)	23.533(2)	12.362(1)
c/Å	47.112(6)	19.570(2)	24.113(2)	16.376(2)
α/°		68.550(7)		98.14(1)
β/°	91.11(1)	72.540(7)	107.56(1)	109.17(1)
γ/°		67.350(7)		108.57(1)
V/Å^3	7529.7(1)	3819.1(7)	9065.9(7)	2104.5(4)
Z	4	4	8	2
Density (calc.)/g cm^{-3}	1.47	1.595	1.531	1.648
Linear absorption coefficient/mm^{-1}	1.24	2.26	1.91	2.07
Crystal volume/mm^3	3.6×10^{-4}	6×10^{-4}	5.1×10^{-3}	2.1×10^{-3}
Crystal color	Dark brown	Dark brown	Dark brown	Dark brown
Diffractometer	Siemens SMART CCD	STOE IPDS	STOE IPDS	STOE IPDS
Temperature/K	300	300	170	300
Radiation, wavelength/Å	Mo K–$L_{(2,3)}$, 0.710 69	Mo K–$L_{(2,3)}$, 0.710 69	Mo K–$L_{(2,3)}$, 0.710 69	Mo K–$L_{(2,3)}$, 0.710 69
Recording 2θ range/°	max. 46.53	2.9–48.4	2.9–48.4	2.9–48.4
Number of exposures/irradiation per exposure (min)	2082/1.5	167/3	111/3	250/4
Refinement conditions				
Number of recorded reflections	43154	30512	54087	16622
Observed independent reflections	6862	4061	5067	3078
Number of variables	478	397	541	272
R_{int} (%)	5.24	4.16	4.5	4.3
Refinement results				
R (%)	6.23	4.8	6.8	6.3
R_w (%)	8.48	5.2	7.8	7.4
S	1.88	0.814	1.340	1.319
Fourier difference/e Å^{-3}	−0.61, 0.76	−0.45, 0.66	−0.40, 0.64	−0.34, 0.56

Table 2 Atomic coordinates and isotropic displacement parameters for the atoms of the $[Ni_3P_3S_{12}]^{3-}$ anions in $(PPh_4)_3[Ni_3P_3S_{12}]$

Atom	x	y	z	$10^2\ U_{eq}/Å^2$
Ni(1)	0.36235(5)	0.52140(8)	0.40430(2)	4.01(3)
Ni(2)	0.37488(5)	0.38064(8)	0.33983(2)	3.86(3)
Ni(3)	0.19590(5)	0.46923(8)	0.36807(2)	3.84(3)
P(1)	0.5189(1)	0.3941(2)	0.38108(3)	4.37(7)
S(11)	0.4363(1)	0.5422(2)	0.36500(3)	4.03(5)
S(12)	0.4608(1)	0.3807(2)	0.41934(3)	5.06(6)
S(13)	0.6411(1)	0.4229(2)	0.38376(4)	6.33(7)
S(14)	0.4832(1)	0.2545(2)	0.35210(4)	5.19(6)
P(2)	0.2084(1)	0.3247(2)	0.31283(3)	4.59(6)
S(21)	0.26295(9)	0.5024(2)	0.32791(3)	4.05(5)
S(22)	0.3187(1)	0.2202(2)	0.31396(4)	5.84(7)
S(23)	0.1466(1)	0.3275(2)	0.27673(4)	7.41(8)
S(24)	0.1370(1)	0.2931(2)	0.34811(4)	5.41(6)
P(3)	0.1920(1)	0.5900(2)	0.42572(3)	4.94(6)
S(31)	0.2545(1)	0.6455(2)	0.38840(3)	4.40(6)
S(32)	0.1218(1)	0.4424(2)	0.40691(4)	5.59(6)
S(33)	0.1255(1)	0.7180(2)	0.44650(5)	8.41(9)
S(34)	0.2996(1)	0.5223(2)	0.44613(4)	5.86(7)

collected in 15 min, which was important for studying the kinetics of the faster reactions. The same species are observed at different concentrations, but the influence of concentration upon the rate of dissolution/rearrangement has not been investigated.

From chains to crowns in organic solution

$KNiPS_4$, $KPdPS_4$ and the series of compounds $KNi_xPd_{1-x}PS_4$ were all found to be soluble in dimethylformamide (DMF) and dimethyl sulfoxide (DMSO), among several other polar solvents investigated. As DMSO does not always allow for easy extraction of soluble products, DMF was used for most studies presented here. $KPdPS_4$ formed a viscous orange solution, but in contrast to the Ni behaviour, heating at 323 K, even for 3 months, did not affect its viscosity or colour. The $KNi_xPd_{1-x}PS_4$ compounds dissolved to form brown viscous solutions, whose viscosity and color changed upon heat treatment. Interestingly, no compounds could be recrystallized directly from a freshly prepared $KMPS_4$–DMF solution. However, if the $KNiPS_4$ solution was heated at 323 K for two days it was possible to obtain crystallised samples after substituting K^+ by an organic cation.

The structure adopted by $KNiPS_4$ and $KPdPS_4$ has already been reported.[23,24] It consists of infinite $[MPS_4]^-$ chains (Fig. 1) aligned in a parallel fashion, which are separated by a van der Waals gap, to form layers that are sandwiched between alkali metal sheets. The one-dimensional chains are built from M centred $[MS_4]$ rectangles and phosphorus-centred $[PS_4]$ tetrahedra that share edges. Thus, in the $[MPS_4]^-$ chains, alternating $[MS_4]$ rectangular planes are rotated by 90° with respect to each other, similar to that encountered in K_2SnTe_5 with Sn and Te in tetrahedral and square planar tellurium environments, respectively.[30]

As exemplified in Fig. 2 for $(PPh_4^+)_3[(NiPS_4^-)_3]$,[25] the series of $(A^+)_3[(NiPS_4^-)_3]$ salts ($A^+ = TEA^+$, TMA^+, MEM^+, PPh_4^+) contain discrete concave, cyclic and trimetallic, trivalent $[Ni_3P_3S_{12}]^{3-}$ entities instead of the infinite chain $^1_\infty[NiPS_4]^-$ of the parent $KNiPS_4$ phase. Remarkably, the single crystal X-ray structure determinations reveal that the four compounds contain the same $[Ni_3P_3S_{12}]^{3-}$ anions, regard-

Table 3 Selected distances (Å) and angles (°) for the $[Ni_3P_3S_{12}]^{3-}$ anion in $(PPh_4)_3[Ni_3P_3S_{12}]$

Rectangular environment of Ni(1):					
Ni(1)–S(11)	2.219(2)	S(11)–S(12)	3.054(2)	S(11)–Ni(1)–S(12)	87.06(6)
Ni(1)–S(12)	2.216(2)	S(11)–S(31)	3.272(2)	S(12)–Ni(1)–S(34)	92.45(7)
Ni(1)–S(34)	2.224(2)	S(12)–S(34)	3.206(2)	S(34)–Ni(1)–S(31)	86.75(7)
Ni(1)–S(31)	2.235(2)	S(31)–S(34)	3.063(2)	S(31)–Ni(1)–S(11)	94.32(6)
Average	2.224(2)				
Rectangular environment of Ni(2):					
Ni(2)–S(11)	2.229(2)	S(11)–S(21)	3.249(2)	S(11)–Ni(2)–S(21)	93.81(6)
Ni(2)–S(21)	2.220(2)	S(11)–S(14)	3.064(2)	S(22)–Ni(2)–S(14)	91.34(7)
Ni(2)–S(22)	2.204(2)	S(21)–S(22)	3.059(2)	S(14)–Ni(2)–S(11)	87.43(6)
Ni(2)–S(14)	2.204(2)	S(14)–S(22)	3.153(2)	S(21)–Ni(2)–S(22)	87.47(7)
Average	2.214(2)				
Rectangular environment of Ni(3):					
Ni(3)–S(21)	2.213(2)	S(31)–S(32)	3.073(2)	S(24)–Ni(3)–S(32)	91.58(7)
Ni(3)–S(24)	2.210(2)	S(31)–S(21)	3.200(2)	S(32)–Ni(3)–S(31)	87.98(7)
Ni(3)–S(32)	2.209(2)	S(32)–S(24)	3.168(2)	S(31)–Ni(3)–S(21)	92.54(6)
Ni(3)–S(31)	2.216(2)	S(21)–S(24)	3.070(2)	S(21)–Ni(3)–S(24)	87.90(6)
Average	2.212(2)				
Tetrahedral environment of P(1):					
P(1)–S(11)	2.118(2)	S(11)–S(12)	3.054(2)	S(11)–P(1)–S(12)	94.43(9)
P(1)–S(12)	2.043(2)	S(11)–S(13)	3.554(2)	S(12)–P(1)–S(13)	114.4(1)
P(1)–S(13)	1.957(2)	S(11)–S(14)	3.064(2)	S(13)–P(1)–S(14)	114.1(1)
P(1)–S(14)	2.036(2)	S(12)–S(13)	3.364(2)	S(14)–P(1)–S(11)	95.04(9)
Average	2.039(2)	S(12)–S(14)	3.439(2)	S(11)–P(1)–S(13)	121.4(1)
		S(13)–S(14)	3.350(2)	S(12)–P(1)–S(14)	115.0(1)
Tetrahedral environment of P(2):					
P(2)–S(21)	2.109(2)	S(21)–S(22)	3.059(2)	S(21)–P(2)–S(22)	95.0(1)
P(2)–S(22)	2.040(2)	S(21)–S(23)	3.486(2)	S(22)–P(2)–S(23)	116.5(1)
P(2)–S(23)	1.946(2)	S(21)–S(24)	3.070(2)	S(23)–P(2)–S(24)	115.8(1)
P(2)–S(24)	2.053(2)	S(22)–S(23)	3.389(2)	S(24)–P(2)–S(21)	95.04(9)
Average	2.037(2)	S(22)–S(24)	3.403(2)	S(21)–P(2)–S(23)	118.5(1)
		S(23)–S(24)	3.387(2)	S(22)–P(2)–S(24)	112.5(1)
Tetrahedral environment of P(3):					
P(3)–S(31)	2.110(2)	S(31)–S(32)	3.073(2)	S(31)–P(3)–S(32)	95.27(9)
P(3)–S(32)	2.050(2)	S(31)–S(33)	3.523(2)	S(32)–P(3)–S(33)	114.0(1)
P(3)–S(33)	1.944(2)	S(31)–S(34)	3.063(2)	S(31)–P(3)–S(33)	120.7(1)
P(3)–S(34)	2.057(2)	S(32)–S(33)	3.350(2)	S(32)–P(3)–S(34)	113.4(1)
Average	2.040(2)	S(32)–S(34)	3.433(2)	S(33)–P(3)–S(34)	115.9(1)
		S(33)–S(34)	3.391(2)	S(34)–P(3)–S(31)	94.6(1)

Table 4 Cell parameters obtained from Rietveld analysis of the solid solutions $KNi_xPd_{1-x}PS_4$ for the three substitutions studied. For $x=0$ and 1, the parameters are from previous structural investigations[23,24]

	x				
	1	0.76(2)	0.44(2)	0.22(3)	0
a/Å	8.2538(4)	8.3010(10)	8.4099(6)	8.4400(9)	8.5337(2)
c/Å	10.7553(6)	10.6900(12)	10.6434(9)	10.6027(10)	10.5595(2)
V/Å^3	732.7(2)	736.6(3)	752.8(2)	755.3(2)	769.0(1)
R_{wp}	—	8.74	9.56	10.9	—
χ^2	—	3.68	4.18	6.87	—

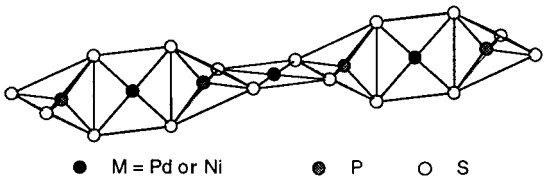

Fig. 1 Part of the infinite $^1_\infty[KMPS_4]^-$ chain in $KMPS_4$ (M = Ni, Pd) showing the alternating $[MS_4]$ rectangles and $[PS_4]$ tetrahedra.

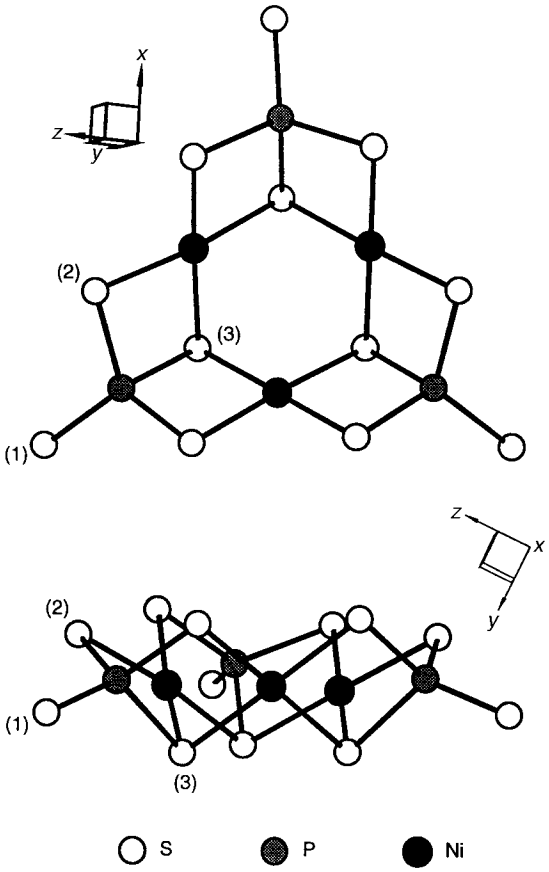

Fig. 2 Bowl-like structure of the $[Ni_3P_3S_{12}]^{3-}$ anions present in the structures of $A_3[(NiPS_4)_3]$ (A = TMA^+, TEA^+, PPh_4^+ and MEM^+). Top: view showing the pseudo three-fold axis and the arrangement of the $[NiS_4]$ rectangles and $[PS_4]$ tetrahedra. Bottom: side view showing the three dangling single-bonded outer sulfur atoms (1), the double-bonded (2), and the triple-bonded (3) interior sulfur environments.

less of the size and shape of the organic template cation (Fig. 3). In that respect, the synthesis of the $[Ni_3P_3S_{12}]^{3-}$ crown appears to follow a very different mechanism when compared to the solution synthesis of metal–halides,[31] metal–ligand systems,[32] and metal–polychalcogenides,[33] for which a strong cation structural dependency has been observed. This novel inorganic cycle consists of nickel in sulfur rectangular planar coordination linked through edge sharing to two $[PS_4]$ tetrahedral groups and through corner sharing to two $[NiS_4]$

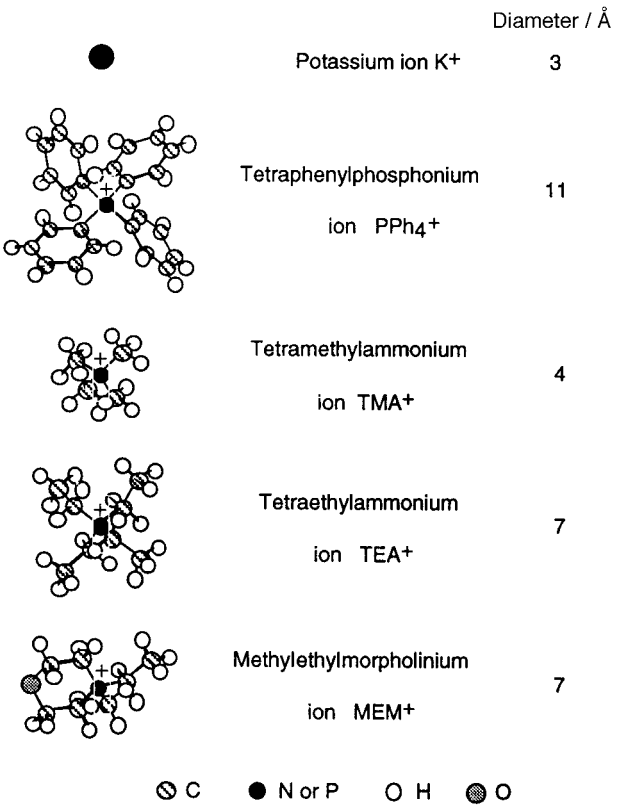

Fig. 3 Diameters of the A cations of the $A_3[(NiPS_4)_3]$ phases (A = TMA^+, TEA^+, PPh_4^+ and MEM^+).

rectangles. Hence, the coordination by sulfur around Ni and P is the same as in the $KNiPS_4$ precursor. The $[Ni_3P_3S_{12}]^{3-}$ anion has a quasi-three-fold symmetry axis so even though the three metal and phosphorus sites are crystallographically inequivalent, they are chemically identical. Three sulfur coordination types are observed. The chalcogen atoms at the bowl periphery are in a $[PS_4]$ tetrahedron and are solely engaged in a single bond with phosphorus. Moving towards the bowl centre, the valency of the sulfur atoms increases. One sulfur is singly bonded to one P and one Ni, and the other sulfur is involved with two bonds to one Ni and one bond to one P.

The average Ni–S distances of 2.217(2), 2.216(2), 2.213(2) and 2.222(5) Å for samples **1, 2, 3** and **4**, respectively, compare well with the mean distance observed in $KNiPS_4$ [2.218(2) Å]. The S–S contacts for the $[NiS_4]$ square may be divided into two groups: (a) short S–S distances for the edges common to $[NiS_4]$ and $[PS_4]$ polyhedra, the average values being 3.064(2), 3.061(6) and 3.058(6) and 3.064(6) Å, respectively, for **1**, **2**, **3** and **4**, and (b) longer distances for the unshared edges [3.208(2), 3.203(6), 3.203(6) and 3.218(6) Å for samples **1**, **2**, **3** and **4**, respectively]. These mean values are comparable to the analogous contacts observed in $KNiPS_4$ of 3.088 and 3.180 Å. Both $KNiPS_4$ and the $ANiPS_4$ phases show $[NiS_4]$ motifs with a sulfur rectangular planar coordination, although

a square configuration was expected: this can be ascribed to a distortion associated with steric as well as electrostatic factors.[34,35]

In contrast to the Ni–S distances that vary very little [from 2.193(5) to 2.235(2) Å for all compounds reported here], changes in the P–S distances are related to the valency of sulfur, and thus three types of P–S distances can be distinguished: (i) the longest P–S distances [2.112(2), 2.114(2), 2.109(2) and 2.121(6) Å (mean values for **1**, **2**, **3** and **4**, respectively)] are encountered for P bound to trivalent chalcogens; (ii) the intermediate P–S distances correspond to interactions of phosphorus with divalent chalcogens [2.047(2), 2.041(6), 2.050(6) and 2.051(6) Å (mean values for **1**, **2**, **3** and **4**, respectively)] and (iii) the shortest P–S distances are those involving the three monovalent sulfur atoms, pointing towards the organic cations [1.949(2), 1.949(2) and 1.948(2) and 1.953(6) (mean values for **1**, **2**, **3** and **4**)]. These sulfide anions have the highest equivalent isotropic atomic displacement parameters in accordance with their low coordination.

Such a dispersion of the P–S distances is commonly encountered in the literature for phosphorus cations surrounded by chemically distinct chalcogens. The higher the sulfur coordination, the larger the P–S distance. Nevertheless, the average P–S distance in $[Ni_3P_3S_{12}]^{3-}$ [2.039(2), 2.035(6), 2.036(6) and 2.042(6) Å for **1**, **2**, **3** and **4**, respectively] remains fairly comparable to the P–S distances observed in $KNiPS_4$ [2.036(2) Å] reflecting the same bonding character in all these phases in relation to their charge.

Electronic structure of the novel ring anion $[(NiPS_4)_3]^{3-}$

Electronic calculations have been performed on the $[Ni_3P_3S_{12}]^{3-}$ anion by employing the extended Hückel tight-binding method.[36,37] A modified Wolfsberg–Helmotz formula was used to calculate the non diagonal $H_{\mu\nu}$ values.[38] The ionization potentials (eV) and exponents used were −20.78 and 2.51 for S 3s, and −13.20 and 2.16 for S 3p, respectively. The organic cation groups were neglected in the calculations. Atomic positions of Ni, P and S were taken from the crystal structure of sample **1**.

As expected, $(PPh_4^+)_3[Ni_3P_3S_{12}]^{3-}$ exhibits an insulator behaviour with a calculated band gap of about 2.6 eV. The LUMO is built upon a high hybridisation of the $d_{x^2-y^2}$ orbital of nickel with the sp orbitals of the $[NiS_4]$ square chalcogen to form a σ* molecular bond. This block of three orbitals (one per Ni atom) is well separated from the sp cationic levels which are 4.5 eV higher in energy. The nature of the HOMO levels are more difficult to assign in view of the high hybridisation of the chalcogen and the nickel orbitals. The last occupied level is essentially based upon π* Ni–S bands, with some non-bonding contributions from all the sulfur atoms. No contribution of phosphorus appears at the proximity of the HOMO–LUMO levels.

When changing from $KNiPS_4$ to $A_3[Ni_3P_3S_{12}]$, no significant modification of the charge balance is expected. Both K and A are assumed to donate one electron to the $[NiPS_4]^-$ entities. In both cases, Ni^{II} and P^V configurations (d^8 low spin and s^0p^0, respectively) are in agreement with the M–S distances and the coordination of their closest S^{-II} anionic neighbours. However, because of the modification of the structural arrangement of the $[PS_4]$ tetrahedra and $[NiS_4]$ rectangles in the $A_3[Ni_3P_3S_{12}]$ compounds the three different sulfur types that occur in these materials should bear three different ionic charges. A more negative charge is expected for a lower coordination and *vice versa*. According to the coordination of the chalcogen atoms, their valence orbitals are engaged in one, two or three σ bonds, the others giving rise to lone pair levels (if π_{Ni-S} bonds are not taken into account). The electronic density of a chalcogen should then increase with the number of lone pair levels. For three-, two- and one-coordinate sulfur atoms, Mulliken analyses yielded charges of *ca.* −0.05, −0.56, and −1.07 e^- per sulfur, respectively. The last value corresponds to the sulfur atoms located on the outside of the bowl; the near zero value being that of the chalcogen atoms inside the cycle. This means that the three negative charges of the $[Ni_3P_3S_{12}]^{3-}$ anions are essentially located at the periphery of the anion (*ca.* 120° from each other). This particular feature should confer a high chemical reactivity upon these anions.

The mean value of $-0.56\ e^-/S$ is comparable to the sulfur charge calculated for $[NiPS_4]^-$ in $KNiPS_4$ ($-0.54\ e^-/S$).[23] Also, the gross populations determined for nickel and phosphorus in $KNiPS_4$ and $(PPh_4^+)_3[Ni_3P_3S_{12}]^{3-}$ are quite similar. Thus, comparing $KNiPS_4$ to $(PPh_4^+)_3[Ni_3P_3S_{12}]^{3-}$, in the latter compound a redistribution of the electronic cloud around the sulfur atoms is observed without alteration of the element mean ionisation states.

Solution phase chemistry of $KNiPS_4$ and $KPdPS_4$

In accordance with their highly anisotropic bonding, the $KMPS_4$ (M = Ni, Pd) compounds are soluble in polar organic solvents rapidly forming highly viscous gel-like solutions at high concentrations ($[KMPS_4] > 10^{-2}$ mol l^{-1}).[39] This solubility is unusual in solid-state chemistry and opens up the way for performing novel chemistry, that can possibly be more readily controlled than usual 'shake and bake' solid-state methods. In addition, complex fluids, including lyotropic mesophases, that can be obtained from solutions of anisotropic mineral motifs dissolved in organic solvents,[22,25,40] can potentially be exploited to produce novel phases with interesting properties, for example magnetically/electrically aligned samples. Consequently, detailed investigations of the $KMPS_4$–DMF solutions are particularly important for understanding why, for example, can crystalline $A_3[Ni_3P_3S_{12}]$ compounds only be synthesised from solutions of $KNiPS_4$–DMF that have been heated for a period of time? When do the bowl-like anions form? Why do not $A_3[Pd_3P_3S_{12}]$ compounds form in a similar way? Why do the colours and textures of the solutions change with time? Is it possible to dissolve the chains without breaking them? The latter question is particularly important as if the chain is soluble and remains sufficiently anisotropic, *i.e.* does not fold, it could be possible to obtain a liquid crystal phase. To try to address these questions we have characterised the solutions using electro-spray mass spectroscopy (ESMS), solution-state ^{31}P NMR and optical microscopy.

Fig. 4 shows the anionic (ES^-) species ESMS spectrum of a DMF–$KNiPS_4$ solution that had been heated at 323 K for

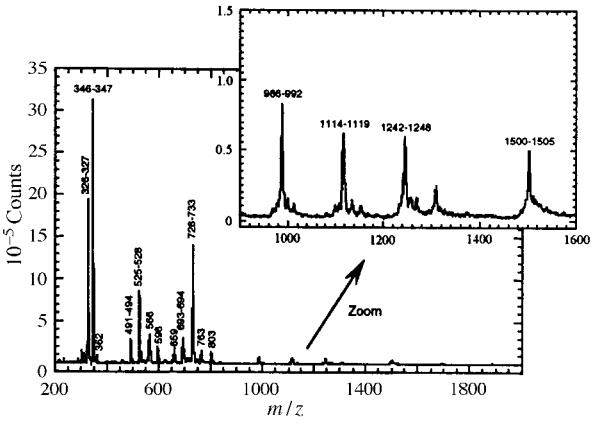

Fig. 4 ES^- ESMS spectrum of a solution of $KNiPS_4$ in DMF that had been heated at 323 K for 5 days. Assignments of the peaks are given in Table 5.

Table 5 Assignments of ES^- peaks in the ESMS spectra of $KNiPS_4$–DMF solutions in Fig. 4

Measured m/z	Species	Calculated m/z and (isotopic %)
326–327	$[(Ni_3P_3S_{12})H]^{2-}$	326(31), 327(36), 328(14)
346–347	$[(Ni_3P_3S_{12})K]^{2-}$	345(31), 346(36), 347(14)
362	$[(Ni_3P_3S_{12})(DMF)H]^{2-}$	362.5(31), 363.5(36), 364.5(14)
693–694	$[(Ni_3P_3S_{12})HK]^-$	691(31), 693(36), 695(14)
728–733	$[(Ni_3P_3S_{12})K_2]^-$	729(31), 731(36), 733(14)
763	$[(Ni_3P_3S_{12})HK(DMF)]^-$	764(31), 766(36), 768(14)
803	$[(Ni_3P_3S_{12})K_2(DMF)]^-$	802(31), 804(36), 806(14)
Weak peaks attributable to decomposition products		
491–494	$[(Ni_3P_2S_9)H]^- - S$	493(31), 495(36), 497(14)
525–528	$[(Ni_3P_2S_9)H]^-$	525(31), 527(36), 529(14)
566	$[(Ni_3P_2S_9)K]^-$	563(31), 565(36), 567(14)
596	$[(Ni_3P_3S_{12})HK]^- - 3S$	595(31), 597(36), 599(14)
659	$[(Ni_3P_3S_{12})HK]^- - S$	659(31), 661(36), 567(14)
1114–1119	$[(Ni_5P_5S_{20})K_4]^- - [PS_3]$	1117
Weak peaks attributable to $[NiPS_4]_n^{n-}$ fragments with $n=4$, 5 and 6		
986–992	$[(Ni_4P_4S_{16})K_3]^-$	987[a]
1242–1248	$[(Ni_5P_5S_{20})K_4]^-$	1244[a]
1500–1505	$[(Ni_6P_6S_{24})K_5]^-$	1500[a]

[a]Mean calculated m/z.

5 days. It consists of a series of sharp peaks that can be assigned (Table 5) in terms of $[Ni_3P_3S_{12}]^{3-}$ anions associated with H^+, K^+ and DMF molecules. The ES^+ mass spectrum (not shown) is in agreement with this as peaks are observed for H^+ and K^+ associated with DMF molecules. Several weak peaks in the ES^- spectrum also appear at m/z values >950. They can be attributed to fragments with sizes larger than $[Ni_3P_3S_{12}]^{3-}$, such as anions containing more than three nickel atoms. As the peaks are rather weak their respective isotopic abundances have not been calculated, only their mean m/z, which are reported in Table 5. The $[NiPS_4]_n^{n-}$ anions with $n=$ 4, 5 and 6 are associated with three, four and five potassium cations, respectively form singly charged entities. At present, there is no structural information about these anions since they have not been isolated in the solid state.

^{31}P NMR experiments were performed on $KNiPS_4$–DMF solutions, similar to those used in the above ESMS studies, prepared by vigorous stirring at 273 K [Fig. 5(a)] and then heated at 323 K for 5 days [Fig. 5(b)]. A single signal in each spectrum is observed at δ 122 and at δ 114, respectively. By comparison with the solid-state ^{31}P NMR spectra of $KNiPS_4$ and $(PPh_4)NiPS_4$, which can be considered as spectroscopic

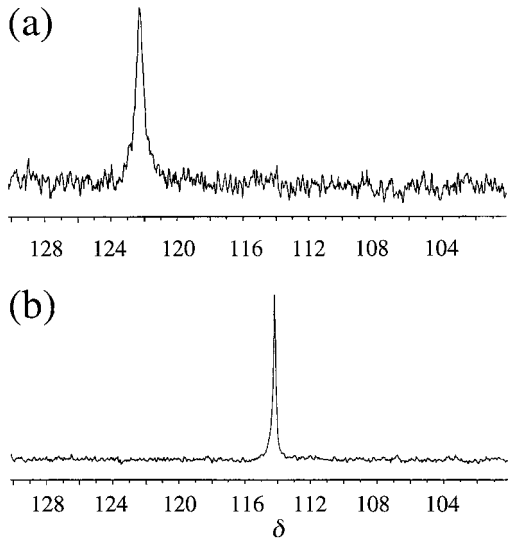

Fig. 5 ^{31}P solution-state NMR spectra of (a) $KNiPS_4$ dissolved in DMF at 273 K and (b) a solution of $KNiPS_4$ in DMF heated at 323 K for 5 days.

references for the chain and the cyclic anions, respectively, it was possible to assign the peak at δ 122 to the chain, $^1_\infty[NiPS_4]^-$ in solution, and the peak at δ 114 to the cyclic anion, $[Ni_3P_3S_{12}]^{3-}$, in solution. $KNiPS_4$, in the solid and solution state, has one resonance in agreement with the one crystallographic site in the chain structure. No magnetic difference is observed corresponding to phosphorous atoms near to, and at the ends of the chains, indicating that, either there is no chemical shift difference between these sites, or more likely, the chains are so long that the relative concentration of the P sites at the end of the chain will be extremely small. Thus, the ESMS and NMR data confirm that the $^1_\infty[NiPS_4]^-$ chain is soluble and remains intact in DMF at low temperature.

The solid-state ^{31}P NMR spectrum of $(PPh_4)NiPS_4$ exhibits three resonances, in addition to the phenyl groups (δ 23.8 and 21.3), at δ 112.6, 109.6, 106.4. These can be assigned to the three crystallographic inequivalent P sites in the $[Ni_3P_3S_{12}]^{3-}$ anion. In solution, rapid thermal motion will ensure that the crystallographic inequivalence will be lost, such that individual resonances will be observed only from magnetically inequivalent species. Hence, the crown in solution has one resonance in the ^{31}P NMR spectrum. Apparently there are no major structural changes of the chain or the crown in solution as the chemical shifts are extremely close to those in the solid state confirming that the $[Ni_3P_3S_{12}]^{3-}$ anion seen in the ESMS study does adopt the same cyclic structure as that observed by X-ray diffraction in the $A_3[Ni_3P_3S_{12}]$ salts. Fig. 5(b) shows that after 5 days at 323 K the signal from the chain has completely disappeared. Also, there is no evidence for other $[NiPS_4]_n^{n-}$ anions with $n=4$, 5 and 6 as observed in the ESMS ES^- spectrum suggesting that these species were produced *in situ* when the solution formed a spray as the ^{31}P NMR spectrum should reflect the change in bond angles between the different cycles.

From the ESMS and NMR data it can be concluded that the chain $^1_\infty[NiPS_4]^-$ is soluble in DMF, but it is thermodynamically unstable and under relatively mild conditions (heating at 323 K for 5 days) it fragments and the cyclic bowl-like anion, $[Ni_3P_3S_{12}]^{3-}$, forms. This is an autofragmentation/rearrangement process that does not require the addition of any large organic cation, and does not arise from the substitution of K^+ by A^+. From these observations the occurrence of $[Ni_3P_3S_{12}]^{3-}$ anions in all the $ANiPS_4$ phases formed from aged $KNiPS_4$–DMF solutions regardless of the size and shape of the A^+ cations (Fig. 3) can be understood. It appears that

this remarkable dispersion/auto-fragmentation/re-arrangement sequence disclosed above extends the concept of mere excision in solution of monomeric molecular motifs from low-dimensional inorganic solids.[41]

In order to determine whether the nature of the solvent can influence the auto-fragmentation of the $^1_\infty[NiPS_4]^-$ chains, an ESMS analysis of a solution of $KNiPS_4$ in dimethyl sulfoxide (DMSO) heated at 323 K for 5 days was also carried out. Again, $[Ni_3P_3S_{12}]^{3-}$ species in association with H^+ and K^+ are observed. Also, the same $[NiPS_4]_n^{n-}$ groups with $n=4$, 5 and 6 are found in minute quantities. Clearly, the use of DMSO with a higher relative permittivity ($\varepsilon=45$ as opposed to 36 for DMF) does not notably change the fragmentation of $KNiPS_4$ chains.

Clearly, the $KNiPS_4$–DMF solution evolves with time at 323 K, but also as described in the synthesis section, visually the solution of $KNiPS_4$ evolves at room temperature, changing colour from dark brown to orange–brown, and progressively becoming more fluid, approaching the solvent fluidity in about 24 h. Thus, the behaviour of the $^1_\infty[KNiPS_4]$ and $^1_\infty[KPdPS_4]$ compounds in solution was investigated by optical microscopy under polarised light. It was observed that when crystals of the solid compounds, placed between a microscope slide and a cover glass, are put into contact with pure DMF, the crystals immediately swell [Fig. 6(a)]. During this process, the small needle shaped crystals that are in suspension rapidly move in the direction of their elongation, and some birefringence is observed in the pathway of the crystals. For the larger crystals where this motion is more hindered, the dissolution is rapidly limited by the diffusion of the molecules in solution away from the crystal, and until all the crystal is dissolved a stationary state remains in which the crystal is surrounded by a birefringent solution.[42] This birefringence decreases as the distance from the crystal increases [Fig. 6(b)]. When the crystal is completely dissolved, the birefringence slowly disappears and within a few minutes, at room temperature, the solution appears isotropic. However, if the solution is now sheared, for example, by translating the cover glass, strong birefringence is immediately observed again. Thus, flow birefringence can be seen for fresh solutions of both $^1_\infty[KPdPS_4]$–DMF and $^1_\infty[KNiPS_4]$–DMF, but in the latter case, as the solution ages at room temperature and becomes more fluid, the intensity of the transient birefringence decreases and finally disappears totally.

Such flow birefringence is commonly observed for solutions of lyotropic mesophases at concentrations slightly under the isotropic/anisotropic transition concentration.[43] Our observation can be explained using two different models: either a preferred orientation of anisotropic rigid molecules induced by flow or by a shock wave, or from stretching of interdigitated, folded, flexible polymers. Both models confirm the existence of $^1_\infty[NiPS_4]^-$ chains in solution for a limited period of time, consistent with the ESMS and NMR data. The loss of flow birefringence can be understood in terms of the chains breaking down into crowns. A transmission electron microscopy study of a dried $KPdPS_4$–DMF solution confirmed that chains remain intact in solution and showed that the chains are flexible, hence favouring the second model.[25]

After establishing that the formation of the $[Ni_3P_3S_{12}]^{3-}$ anions was exclusively a solvent-induced reaction, a study of the kinetics of the fragmentation–rearrangement process of the $[NiPS_4]^-$ chains from a freshly prepared $KNiPS_4$ solution was carried out. A sample of $KNiPS_4$ dissolved in DMF at 273 K was placed into the NMR probe in the bore of the magnet, which had been previously heated to 300 K, and ^{31}P spectra were collected every 15 min. The evolution of the spectrum is shown in Fig. 7. It can be seen that initially the chain anion exists in solution (peak at δ 122), and with time, this is gradually converted to the cyclic trimer anion (δ 114). After 60 h, the conversion is complete. Superimposed upon the kinetics of conversion is the dissolution of the remaining starting material, thus the overall intensity of the spectra increases with time. No other peaks were observed indicating that the breaking of the chains is the rate-limiting process in the formation of the cyclic anion, and any small fragments of chain are consumed rapidly. In addition, we observed that there is a dramatic influence of temperature upon the conversion of chain to crown: at 320 K the conversion is complete after just 12 h.

As discussed previously, $KPdPS_4$ is also soluble in polar solvents, but does not exhibit the same chemical reactivity as $KNiPS_4$. In order to understand this behaviour the mass spectrum of a DMF–$KPdPS_4$ solution was heated at 333 K for 15 h. The resulting ESMS spectrum is shown in Fig. 8. A wide distribution of m/z is observed between 500 and 1100.

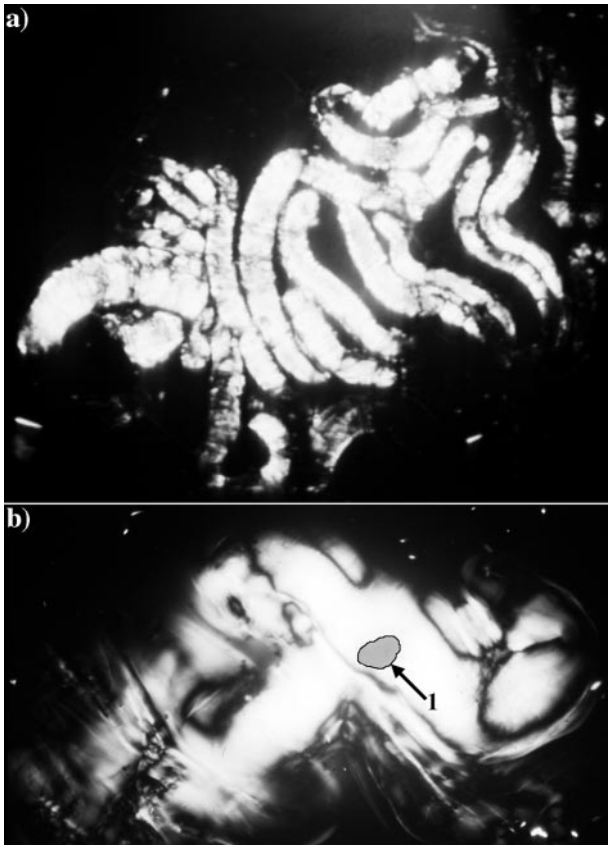

Fig. 6 Transient birefringence observed under polarized light using an optical microscope (width of the image *ca.* 0.5 mm) (a) when crystals of $KMPS_4$ swell giving rise to worm-like textures; (b) for a large single crystal, the zone marked **1** corresponds to the remaining crystal.

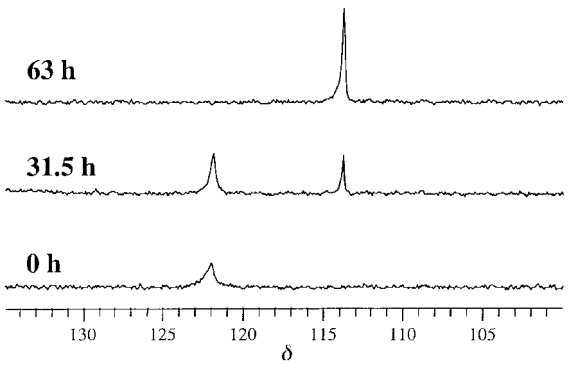

Fig. 7 Evolution of the ^{31}P NMR spectrum of $KNiPS_4$ in DMF prepared at 273 K and then heated *in situ* at 300 K for the times indicated. The concentration of chains in solution initially increases owing to their higher solubility at 300 K.

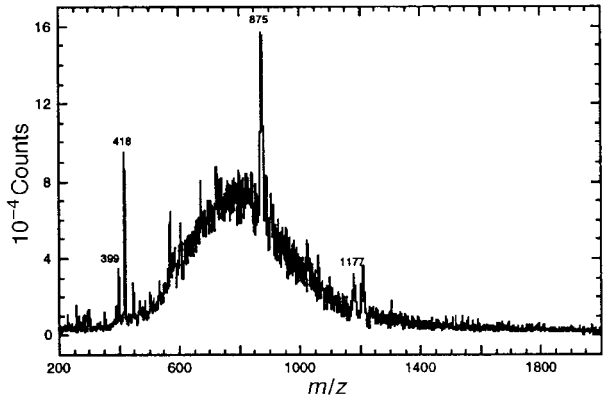

Fig. 8 ES^- ESMS spectrum of $KPdPS_4$ in DMF heated at 333 K for 15 h.

This is characteristic of chains in solution having a distribution of length. Several weak, but sharp, peaks are superimposed upon this background, of which the four most intense can be assigned to: $[(Pd_3P_3S_{12})H]^{2-}$ (*m/z* 399), $[(Pd_3P_3S_{12})K]^{2-}$ (*m/z* 418), $[(Pd_3P_3S_{12})K_2]^-$ (*m/z* 875) and $[(Pd_4P_4S_{16})K_3]^-$ (*m/z* 1117). However, by comparing the intensity scales of Fig. 4 and 8 it can be seen that the concentration of $[Pd_3P_3S_{12}]^{3-}$ relative to $[Ni_3P_3S_{12}]^{3-}$ is extremely small. The ^{31}P NMR spectrum of a $KPdPS_4$–DMF solution prepared at room temperature, contains one resonance at δ 146.9, which is close to the peak at δ 149 observed by solid-state ^{31}P NMR from the $KPdPS_4$ sample itself, again, consistent with the existence of Pd chains in solution. The solution also shows strong flow birefringence, and in contrast to $KNiPS_4$, this does not diminish with time at room temperature.

The $KPdPS_4$ chains in DMF solution are considerably more stable than $KNiPS_4$ chains. Even after heating the former solution at 323 K for 15 days the ESMS spectrum remained unchanged. This difference in reactivity between the palladium and nickel phases towards the solvent-induced auto-fragmentation may be rationalised in part by the strength of the metal–sulfur bond. IR and Raman spectroscopic measurements and the corresponding valence force field calculations[44,45] have yielded two very different M–S force constants in the two compounds. The calculated values are 75 and 90 N m^{-1} for the Ni–S and Pd–S stretching force constants in accordance with the Pauling electronegativity scale, which would predict an increase in covalency of the M–S bond when Ni is substituted by Pd.

As the Pd–S bond appears much more difficult to break than the Ni–S bond, it was thought that a succession of Pd and Ni cations in the same chain could induce the formation of smaller $[PdPS_4]_n^{n-}$ groups, such as $[Pd_3P_3S_{12}]^{3-}$ anions. Thus, three compounds of the type $KNi_xPd_{1-x}PS_4$ where $x=$ 0.22(3), 0.43(2) and 0.76(2) were synthesized. Both results indicate that the $KNi_xPd_{1-x}PS_4$ series of compounds formed solid solutions, where Ni and Pd are completely disordered, which is expected as Ni^{II} and Pd^{II} cations have the same charge and coordination stability.

The ESMS ES^- spectra of the solid solutions $KNi_xPd_{1-x}PS_4$, dissolved in DMF by heating at 333 K for 15 h, are shown in Fig. 9(a)–(c), respectively. The peak assignments are given in Table 6, which show the solutions consist essentially of the anions $[Ni_3P_3S_{12}]^{3-}$, $[Ni_2PdS_{12}]^{3-}$ and $[NiPd_2P_3S_{12}]^{3-}$. Surprisingly, no $[Pd_3P_3S_{12}]^{3-}$ species can be detected in any of the samples, although for the $x=0.22(3)$ solution, a broad background peak can be observed between *m/z* 500–1100, which is similar to that for the $KPdPS_4$ solution, indicating that chains of various lengths exist in solution. Fig. 10 shows the relationship between the intensities of the $[Ni_3P_3S_{12}]^{3-}$, $[Ni_2PdS_{12}]^{3-}$ and $[NiPd_2P_3S_{12}]^{3-}$ peaks and

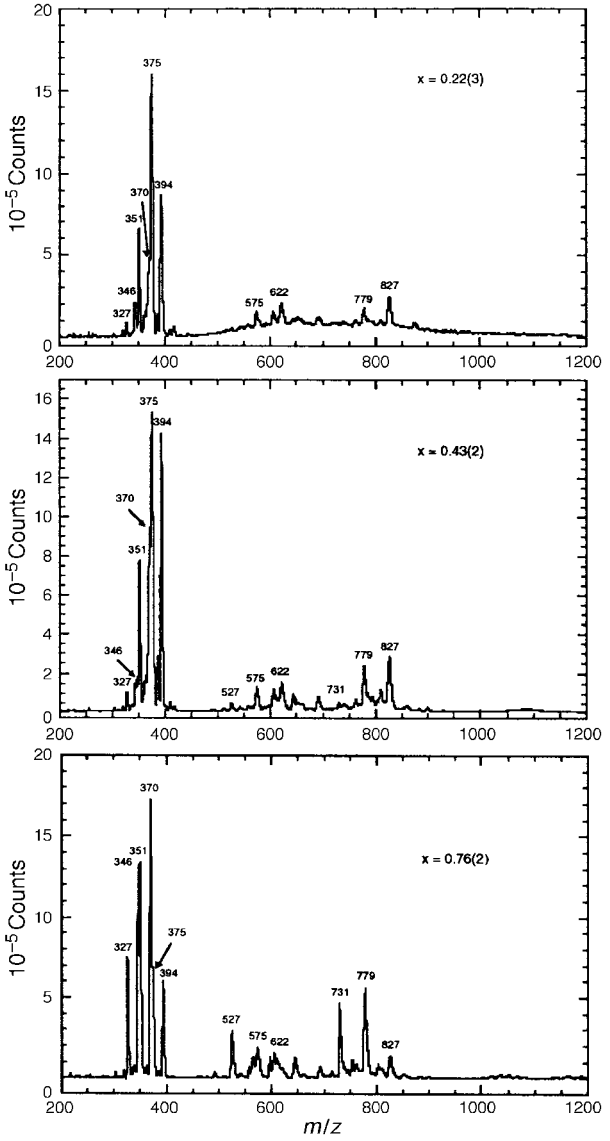

Fig. 9 ES^- ESMS spectra of $KNi_xPd_{1-x}PS_4$ samples dissolved in DMF and heated at 333 K for 15 h, (a) $x=0.22(2)$, (b) 0.43(2) and (c) 0.76(2). Peak assignments are given in Table 6.

Table 6 Assignments of the peaks observed in the ES^- ESMS spectra shown in Fig. 9(a)–(c) of the DMF solutions of $KNi_xPd_{1-x}PS_4$ previously heated at 333 K for 15 h

Measured *m/z*	Species	Peak intensities/10^{-4} counts		
		$x=0.76(2)$	$x=0.43(2)$	$x=0.22(3)$
327	$[(Ni_3P_3S_{12})H]^{2-}$	83.5	11.6	5.8
346	$[(Ni_3P_3S_{12})K]^{2-}$	150.0	18.9	14.5
351	$[(Ni_2PdP_3S_{12})H]^{2-}$	157.7	80.0	45.1
370	$[(Ni_2PdP_3S_{12})K]^{2-}$	180.9	107.6	33.4
375	$[(NiPd_2P_3S_{12})H]^{2-}$	81.9	171.5	109.0
394	$[(NiPd_2P_3S_{12})K]^{2-}$	69.6	157.0	56.7
527	$[(Ni_3P_2S_9)H]^-$	34.0	4.4	~0
575	$[(Ni_2PdP_2S_9)H]^-$	20.1	13.1	7.3
622	$[(NiPd_2P_2S_9)H]^-$	4.6	17.4	10.2
731	$[(Ni_3P_3S_{12})K_2]^-$	51.0	4.4	~0
779	$[(Ni_2PdP_3S_{12})K_2]^-$	58.8	26.2	8.7
827	$[(NiPd_2P_3S_{12})\ K_2]^-$	13.9	27.6	14.5

the *x* value of the starting material. As expected, the concentrations of $[Ni_2PdP_3S_{12}]^{3-}$ and $[Ni_3P_3S_{12}]^{3-}$ species, the richest in nickel, increase with increased Ni content. Fig. 9 also shows that the $KNi_xPd_{1-x}PS_4$ materials consist of disordered $[Ni_xPd_{1-x}PS_4]^-$ chains rather than being a mixture of dis-

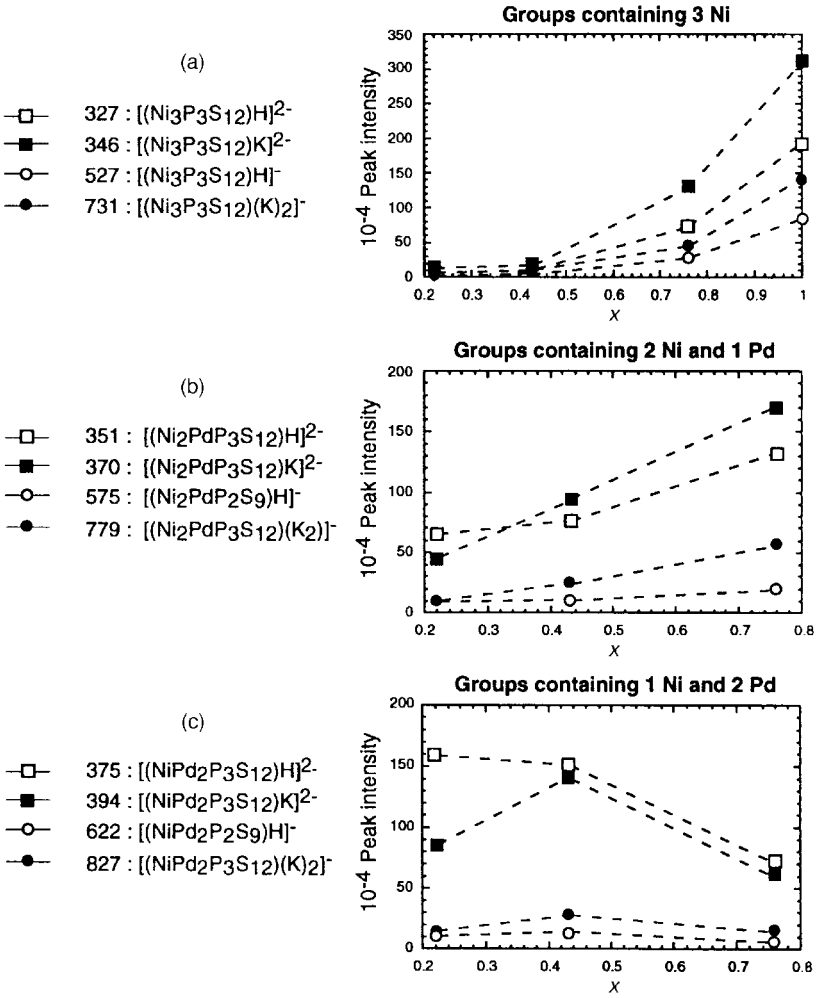

Fig. 10 Peak intensities for the species (a) $[Ni_3P_3S_{12}]^{3-}$, (b) $[Ni_2PdP_3S_{12}]^{3-}$, (c) $[NiPd_2P_3S_{12}]^{3-}$ *vs.* the composition x of $KNi_xPd_{1-x}PS_4$. Data extracted from Fig. 9.

ordered, separated $x[NiPS_4]^-$ and $(1-x)[PdPS_4]^-$ chains, as in this latter case the $[PdPS_4]^-$ chains would not fragment, and we would essentially observe only the formation of the $[Ni_3P_3S_{12}]^{3-}$ entities.

Acknowledgement

This work was supported by the CNRS. L.M.B. thanks the Région Pays de Loire and the CNRS for a post-doctoral fellowship and a visiting scientist grant, respectively.

References

1 *Electronic Properties of Inorganic Quasi-one-dimensional Compounds*, ed. P. Monceau, *Physics and Chemistry of Materials with Low-dimensional Structures Series B*, D. Reidel, Dordrecht, Holland, 1985, parts 1 and 2.
2 *Crystal Chemistry and Properties of Materials with Quasi-one-dimensional Structures*, ed. J. Rouxel, *Physics and Chemistry of Materials with Low-dimensional Structures Series B*, D. Reidel, Dordrecht, Holland, 1986.
3 J. A. Wilson, F. J. DiSalvo and S. Mahajan, *Adv. Phys.*, 1975, **24**, 117.
4 J. A. Wilson, *Phys. Rev. B.*: *Condens. Matter*, 1979, **19**, 6456.
5 *Charge Density Waves in Solids*, ed. L. P. Gor'kov and G. Grüner, Elsevier, Amsterdam, Holland, 1989.
6 F. R. Gamble, F. J. DiSalvo, R. A. Klemm and T. H. Geballe, *Science*, 1970, **168**, 568.
7 Y. Ishihara and I. Nakada, *Solid State Commun.*, 1980, **33**, 385.
8 L. J. de Jongh and A. R. Miedema, *Adv. Phys.*, 1974, **23**, 1.
9 M. Steiner, J. Villain and C. G. Windsor, *Adv. Phys.*, 1976, **25**, 87.
10 J. Rouxel, in *Supramolecular Architecture, Synthetic Control in Thin Films and Solids*, ed. T. Bein, ACS Symp. Ser. 499, American Chemical Society, Washington DC, 1992, p. 88.
11 J. Rouxel, *Adv. Synth. React. Solids*, 1994, **2**, 27.
12 A. Wold, W. Kunmann, R. J. Arnott and A. Feretti, *Inorg. Chem.*, 1964, **3**, 545.
13 C. Fouassier, C. Delmas and P. Hagenmuller, *Mater. Sci. Eng.*, 1977, **31**, 97.
14 S. A. Sunshine, D. Kang and J. A. Ibers, *J. Am. Chem. Soc.*, 1987, **109**, 6202.
15 M. G. Kanatzidis and A. C. Sutorik, *Prog. Inorg. Chem.*, 1995, **43**, 151.
16 M. G. Kanatzidis, *Curr. Opin. Solid State Mater. Sci.*, 1997, **2**, 139.
17 W. Bronger and P. Müller, *J. Less-Comm. Met.*, 1984, **100**, 241.
18 S.-P. Huang and M. G. Kanatzidis, *Inorg. Chem.*, 1991, **30**, 1455.
19 Y.-J. Lu and J. A. Ibers, *Comments Inorg. Chem.*, 1993, **14**, 229.
20 S. S. Dhingra and R. C. Haushalter, *Chem. Mater.*, 1994, **6**, 2376.
21 A. J. Jacobson, in *Soft Chemistry Routes to New Materials*, ed. J. Rouxel, M. Tournoux and R. Brec, Trans Tech Publications Ltd, Aedermannsdorf, Switzerland, Materials Science Forum, vol. 152–153, 1994, p. 1.
22 P. Davidson, J. C. Gabriel, A. M. Levelut and P. Batail, *Europhys. Lett.*, 1993, **21**, 317.
23 (*a*) S. H. Elder, A. Van der Lee, R. Brec and E. Canadell, *J. Solid State Chem.*, 1995, **116**, 107; (*b*) 1995, **117**, 432.
24 K. Chondroudis, M. G. Kanatzidis, J. Sayettat, S. Jobic and R. Brec, *Inorg. Chem.*, 1997, **36**, 5859.
25 J. Sayettat, L. M. Bull, J.-C. P. Gabriel, S. Jobic, F. Camerel, A.-M. Marie, M. Fourmigué, P. Batail, R. Brec and R.-L. Inglebert, *Angew. Chem., Int. Ed. Engl.*, 1998, **37**, 1711.
26 G. M. Sheldrick, SHELXTL™ version 5, Siemens Analytical X-Ray Instruments, Inc., Madison, WI.
27 A. Altomare, G. Cascarano, C. Giacovazzo, A. Guagliardi, M. C. Burla, G. Polidori and M. Camalli, *J. Appl. Crystallogr.*, 1994, **27**, 435.

28 *Xtal3.4 User's Manual*, ed. S. R. Hall, G. S. D. King and J. M. Stewart, Universities of Western Australia, Lamb, Perth, 1995.
29 J. Rodriguez-Carjaval, *Fullprof Manual*, ILL Report, 1992.
30 B. Eisenmann, H. Schwerer and H. Schaefer, *Mater. Res. Bull.*, 1983, **18**, 383.
31 (*a*) S. Andersson, M. Hakansson and S. Jagner, *Inorg. Chim. Acta*, 1993, **209**, 195; (*b*) S. Andersson and S. Jagner, *Acta Chem. Scand. Ser. A*, 1988, **42**, 691; (*c*) 1987, **41**, 230; (*d*) 1986, **40**, 52; (*e*) S. Jagner, S. Olson and R. Stomberg, *ibid.*, 1986, **40**, 230; (*f*) S. Andersson and S. Jagner, *ibid.*, 1986, **40**, 210; (*g*) 1985, **39**, 423; (*h*) 1985, **39**, 799; (*i*) 1985, **39**, 515; (*j*) M. Asplund, S. Jagner and M. Nilsson *ibid.*, 1985, **39**, 447; (*k*) S. Andersson and S. Jagner, *ibid.*, 1985, **39**, 181; (*l*) 1985, **39**, 177; (*m*) M. Asplund and S. Jagner, *ibid.*, 1985, **39**, 47.
32 S. Pohl, R. Lotz, W. Saak and D. Haase, *Angew. Chem.*, *Int. Ed. Engl.*, 1989, **28**, 344.
33 $[Ag(Se_x)]_n^{n-}$ phases were synthesized from a DMF solution of Ag^+ and Se_x^{2-} with an organic cation: M. G. Kanatzidis and S.-P. Huang, *Angew. Chem.*, *Int. Ed. Engl.*, 1989, **28**, 1513.
34 N. Gupta, D.-K. Seo, M.-H. Whangbo, S. Jobic, J. Rouxel and R. Brec, *J. Solid State Chem.*, 1997, **128**, 181.
35 J. Sayettat, P. Deniard, S. Jobic, R. Brec and C. Sourisseau, in preparation.
36 M.-H. Whangbo and R. Hoffmann, *J. Am. Chem. Soc.*, 1978, **100**, 6093.
37 R. Hoffmann, *J. Chem. Phys.*, 1963, **39**, 1397.
38 J. H. Ammeter, H.-B. Bürgi, J. Thibeault and R. Hoffmann, *J. Am. Chem. Soc.*, 1978, **100**, 3686.
39 $KMPS_4$ compounds are miscible at all concentrations with DMF. Highly viscous gels (resembling modelling clay) have been obtained at concentrations as high as 2.2 mol l^{-1} ($KMPS_4$, 6 DMF).
40 (*a*) P. Davidson, J.-C. Gabriel, A.-M. Levelut and P. Batail, *Adv. Mater.*, 1993, **5**, 665; (*b*) J.-C. P. Gabriel, C. Sanchez and P. Davidson, *J. Phys. Chem.*, 1996, **100**, 11139; For a review, see: P. Davidson, P. Batail, J.-C. P. Gabriel, J. Livage, C. Sanchez and C. Bourgaux, *Prog. Polym. Sci.*, 1997, **22**, 913.
41 S. C. Lee and R. H. Holm, *Angew. Chem.*, *Int. Ed. Engl.*, 1990, **29**, 840.
42 The difference between the crystal and the solution can be readily determined by uncrossing the polarizers, which reveals a crystal surrounded by a particle free phase, flowing when compressed, confirming its fluid nature.
43 G. Champetier and L. Monnerie, in *Introduction à la chimie macromoléculaire*, Masson, Paris, 1969, pp. 351–365; S. Chandrasekhar, in *Liquid Crystals*, Cambridge University Press, Cambridge, 1992, pp. 69–71.
44 C. Sourisseau, R. Cavagnat, M. Fouassier, R. Brec and S. H. Elder, *Chem. Phys.*, 1995, **195**, 351.
45 C. Sourisseau, R. Cavagnat, M. Fouassier, J. Sayettat, S. Jobic and R. Brec, in preparation.

Paper 8/05807E